Journal of Ceramic Processing Research. Vol. 22, No. 5, pp. 543~546 (2021)
(Received 14 March 2021, Received in revised form 21 July 2021, Accepted 28 August 2021)
https://doi.org/10.36410/jcpr.2021.22.5.543

J O U R N A L O F
Ceramic Processing Research

Research on grain composition, grain size and electrical conductivity of the $CuCr_{1-x}Mg_xO_2$ ($0 \leq x \leq 0.08$)

Yanyan Tang[a,b], Yiding Hu[a], Yi Li[a], Haorong Wu[a], Liangwei Chen[a] and Lan Yu[a,*]
[a]*Faculty of Material Science and Engineering, Kunming University of Science and Technology, Kunming, Yunnan, 650093, P.R. China*
[b]*Faculty of physics and photoelectric engineering, Weifang University, Weifang, Shandong, 261061, P.R. China*

A series of layered $CuCr_{1-x}Mg_xO_2$ ($0 \leq x \leq 0.08$) polycrystalline ceramics were prepared. The effects of substituting Mg^{2+} cations for Cr^{3+} cations on the grain composition, grain size, grain quantity, and electrical conductivity were investigated. When x = 0–0.04, the distinct layered structure grain grew rapidly with the increase of magnesium in the composition, and the average grain size increased from 2.5 μm (x = 0) to 15 μm (x = 0.04) due to the decrease of activation energy. Furthermore, the bulk density and lattice constant also reached the maximum and minimum values of 4.367 g/cm^3 and 17.083 respectively at x = 0.04. When x = 0.05–0.08, the average grain size slightly decreased due to the grown-up second-phase $MgCr_2O_4$ hindering of grain growth. The results showed that the average size of the second-phase $MgCr_2O_4$ had reached 1.3 μm when x = 0.04. In general, the larger the grain size of polycrystalline ceramics, the more defects in the grain boundaries, and the better its electrical conductivity. Therefore, the solid-phase reaction, which can obtain larger grain size and more grain boundary defects, was chosen here to prepare $CuCr_{1-x}Mg_xO_2$ polycrystalline ceramics, so as to obtain a highly conductive $CuCr_{1-x}Mg_xO_2$ ceramic material. The minimum resistivity of the obtained $CuCr_{0.6}Mg_{0.4}O_2$ polycrystalline ceramic is only 0.091 Ω·cm, which is of great significance for the development of transparent conductive oxides.

Keywords: $CuCr_{1-x}Mg_xO_2$ grain composition grain size grain quantity electrical conductivity.

Introduction

Since the discovery of p-type $CuCr_{1-x}Mg_xO_2$ materials, studies have primarily focused on their thermoelectric, photoelectric, and catalytic properties [1-7], while the crystal structure of $CuCr_{1-x}Mg_xO_2$ and the second phase have been less frequently studied. As a p-type transparent conductive oxide, $CuCr_{1-x}Mg_xO_2$ ceramics have been prepared by hydrothermal synthesis, solid-state reaction, et al. [1, 4, 5, 7, 8], and $CuCr_{1-x}Mg_xO_2$ films have been prepared by reactive magnetron sputtering deposition, sol-gel processing, ALD (atomic layer deposition), et al. [3, 9, 10]. Maignan et al. [1] obtained the microstructure images of $CuCr_{1-x}Mg_xO_2$ ceramics and measured its composition using energy-dispersive X-ray spectroscopy. Yu et al. [3] obtained the microstructure images of $CuCr_{1-x}Mg_xO_2$ films and analyzed their surface topography, root mean square roughness, and optical and electrical properties. Kaya et al. [4] compared the images, resistivity and calculated particle-size distributions of Mg- and Fe-doped $CuCrO_2$ nanocrystals prepared by hydrothermal synthesis. Furthermore, Okuda et al. published a series of research papers on the properties of doped $CuCrO_2$ ceramics [5, 7 ,8]. H.-Y. Chen et al. [9] analyzed the morphologies, and the optical, electrical properties. In this paper, we summarized the statistical grain distribution of the main-phase $CuCr_{1-x}Mg_xO_2$ and second-phase $MgCr_2O_4$ based on electron microscope images. Moreover, we analyzed the characteristics of the grain structure and its correlation with electrical resistivity.

*Corresponding author:
Tel : +18987169597
E-mail: yulan000@hotmail.com

Experiment

The $CuCr_{1-x}Mg_xO_2$ ceramic samples were prepared in two steps using a standard solid-state reaction in air. First, the raw materials (Cu_2O [99.9%], Cr_2O_3 [99.95%], and MgO [99.99%]) were weighed according to the stoichiometric ratio, mixed well, and ground. Then, the powders were pressed into pellets and pre-sintered at 1,100 °C for 12 h. In the second step, the sintered pellets were ground and pressed into pellets again, sintered at 1,100 °C for 12 h, and finally, cooled to room temperature.

The polycrystalline structures of the obtained samples were characterized by BDX3200 X-ray diffraction (XRD). The microstructures were observed using an XL30E scanning electron microscope (SEM). The resistivity-temperature (ρ–T) curves were studied using the four-probe method between 100 and 300 K.

Results and Discussion

Phase structure

The XRD patterns of $CuCr_{1-x}Mg_xO_2$ (x = 0, 0.005, 0.01, 0.02, 0.03, 0.04, 0.05, 0.08) are shown in Fig. 1(a). The figure shows that bulk ceramics comprise a 3R-delafossite structure and a high c-axis orientation. Compared to the $CuCrO_2$ standard spectrum (PDF 89-0539), the strongest (006) diffraction peaks indicate a shift to the right. This implies that the lattice parameter *c* has a decreasing trend. In addition, The spinel phase of $MgCr_2O_4$ with a (311) peak at $2\theta = 35.674^o$ was detected in some of the samples (x = 0.04–0.08). These results are in good agreement with existing studies [5, 6]. Fig. 1(b). shows the relationship between bulk density, lattice parameter *c* and the magnesium doping amount x. As you can see from the Fig. 1(b), substituting magnesium for chromium will produce more crystallizable $CuCr_{1-x}Mg_xO_2$ phase. With the increase of the doping amount of magnesium, the bulk density displayed an increasing trend, while the lattice constant displayed a decreasing trend. When x = 0.04, the bulk density and lattice constant reached the maximum and minimum values of 4.367 g/cm^3 and 17.083 respectively, which is consistent with the reports [1, 11]. This may be mainly due to the saturation of magnesium doping.

Vertical section morphology observation

Scanning electron microscope (SEM) images of $CuCr_{1-x}Mg_xO_2$ samples are shown in Fig. 2. As you can see from the Fig. 2, all samples have layered grains. At a low doping level ($x \leq 0.04$), small grains are loosely distributed and sufficiently grow in the *ab*-plane with a reduction in grain boundaries and pores; At a high doping level (x = 0.05 and 0.08), the grains size and grain boundaries hardly changed. Similar results have previously been reported for Fe- and Mg-doped $CuCrO_2$ nanocrystals [4]. At the same time, the doping of magnesium also introduces the second phase of $MgCr_2O_4$ spinel [1]. When x = 0.005–0.03, fine second-phase $MgCr_2O_4$ grains are observed among the $CuCr_{1-x}Mg_xO_2$ grains; When x = 0.04–0.08, $MgCr_2O_4$ grains have obviously grown in size and reach maximum average value at x = 0.08.

In order to quantitatively describe the crystallization of the $CuCr_{1-x}Mg_xO_2$ samples. The grain size and quantity of $CuCr_{1-x}Mg_xO_2$ phase and $MgCr_2O_4$ phase are counted. Fig. 3 shows the grain size distribution of $CuCr_{1-x}Mg_xO_2$ ($0 \leq x \leq 0.08$) samples. As you can see from Fig. 3, the average grain size is about 2.5 μm at low doping (x = 0, 0.005, 0.01), increase to 15 μm at moderate doping (x = 0.02, 0.03, 0.04), and fall to 11

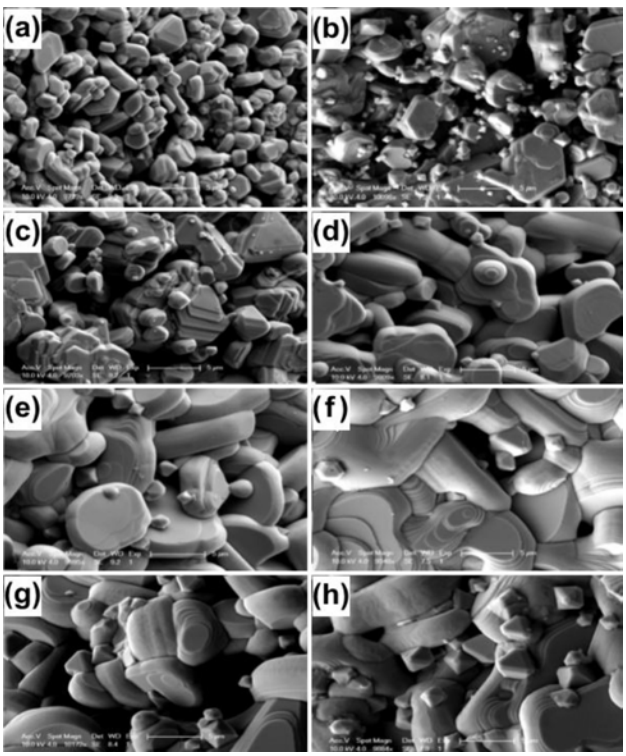

Fig. 2. SEM image of $CuCr_{1-x}Mg_xO_2$ samples: (a) x = 0; (b) x = 0.005; (c) x = 0.01; (d) x = 0.02; (e) x = 0.03; (f) x = 0.04; (g) x = 0.05; and (h) x = 0.08.

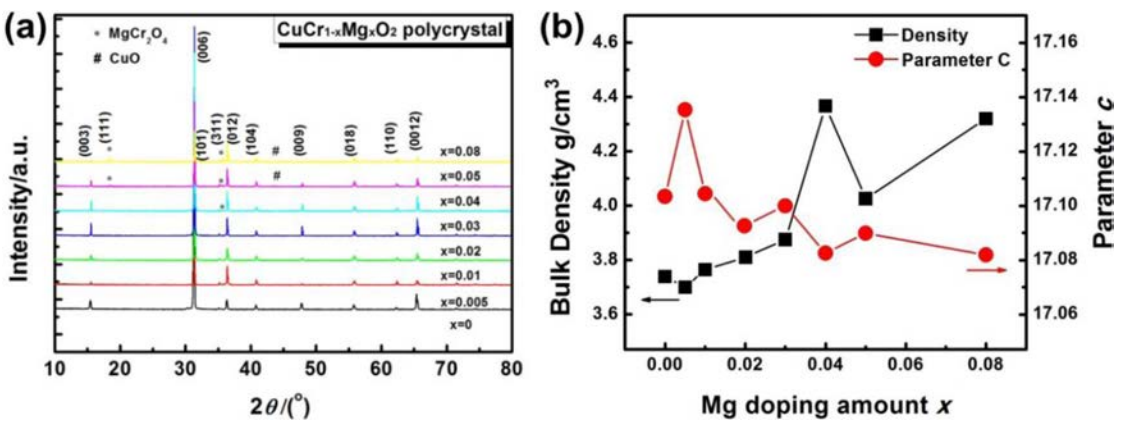

Fig. 1. (a) XRD patterns of $CuCr_{1-x}Mg_xO_2$; (b) relationship between bulk density, lattice parameter and the magnesium doping amount.

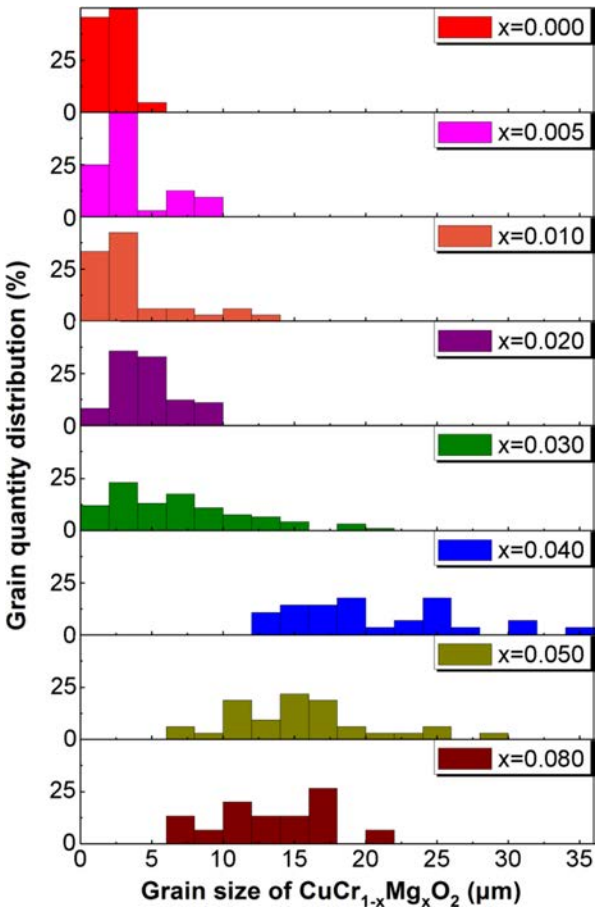

Fig. 3. Grain size distribution of $CuCr_{1-x}Mg_xO_2$ ($0 \le x \le 0.08$) samples

μm at high doping (x = 0.05, 0.08). When x = 0.04, the average size of $CuCr_{1-x}Mg_xO_2$ phase reaches maximum value (15 μm). Further, in order to clarify the reasons for affecting the grain size distribution of the main-phase $CuCr_{1-x}Mg_xO_2$, the associated second-phase $MgCr_2O_4$ was studied. Fig. 4 shows the grain quantity of $MgCr_2O_4$ phase. As you can see from Fig. 4, although the grain quantity is the largest when x = 0.005, the average grain size is only about 0.8 μm, which hardly hinders

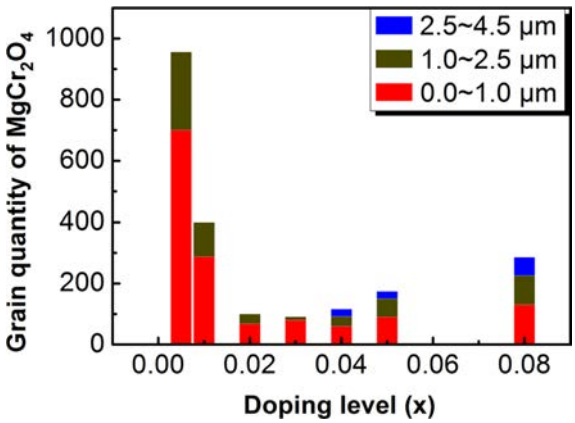

Fig. 4. Grain quantity of $MgCr_2O_4$ phase.

the growth of $CuCr_{1-x}Mg_xO_2$ grains. But when x = 0.04, the average size of the second-phase $MgCr_2O_4$ has reached 1.3 μm, and the hindrance to the average grain size of $CuCr_{1-x}Mg_xO_2$ gradually appears. We speculate that this may be the reason why $CuCr_{1-x}Mg_xO_2$ phase has the largest size when x = 0.04. In addition, this may be the reason why the bulk density and lattice constant reached extreme when x = 0.04. This follows the kinetic grain-growth equation, $G_n - G_0^n = At \exp(-(Q/RT))$, and it is in good agreement with existing reports [12-14]. Changes in the apparent activation energy Q and kinetic grain-growth exponent n in $CuCr_{1-x}Mg_xO_2$ with increase of the magnesium content are thought to be responsible for the crystalline grains size distribution. As the main-phase $CuCr_{1-x}Mg_xO_2$ increases, the acute angles of the grains turned into obtuse angles, indicating a decrease in the crystalline melting point and the liquid precipitation of the polycrystalline grains, which can explain the reason for the increase of $CuCr_{1-x}Mg_xO_2$ grain size too.

Electric transport properties

Fig. 5 shows the resistivity-temperature (ρ-T) curves of $CuCr_{1-x}Mg_xO_2$ ($0.01 \le x \le 0.08$) polycrystals. The resistivity is measured by a four-probe method and the

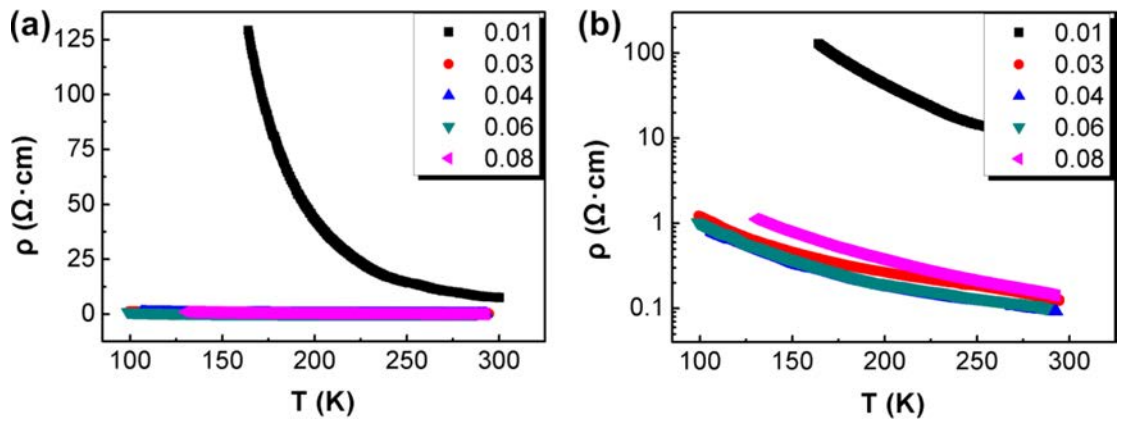

Fig. 5. ρ-T curves of $CuCr_{1-x}Mg_xO_2$ ($0.01 \le x \le 0.08$) polycrystals: (a) linear ordinate; (b) logarithmic ordinate.

Table 1. The room-temperature resistivity of $CuCr_{1-x}Mg_xO_2$

Compound	Maximum substitution level (x)	Resistivity (Ω·cm)	Avarage grain size	Prepared method	References
$CuCr_{1-x}Mg_xO_2$	0.03	68	10 nm	hydrothermal synthesis	[4]
	0.03	1.1	2 μm	self-combustion urea nitrate process	[16]
	0.03	0.1	20 μm	standard solid-state reaction	[15]
	0.04	0.091	15 μm	standard solid-state reaction	This work

resistivity is calculated by formula for volume resistivity ($\rho = RS/L$, where R is the resistance, S is the area, and L is the length). All the samples show semiconducting electrical transport behavior. When x = 0–0.04, the resistivity rapidly decreases with the increase of magnesium doping amount. The room-temperature resistivity reaches a minimum of 0.091 Ω·cm at x = 0.04, which is comparable to the results of existing reports shown in Table 1 [4, 15, 16]. When x = 0.05–0.08, the resistivity is almost unchanged. This is because the grain size reaches its highest level, resulting in the best integrity of the lattice at x = 0.04. Thus, the reduction of grain boundaries may also have been responsible for the decrease in resistivity.

Conclusion

In this study, $CuCr_{1-x}Mg_xO_2$ ($0 \le x \le 0.08$) polycrystalline ceramics were prepared using a solid-state reaction. And the effects of magnesium doping on lattice constant c, bulk density, average grain size, resistivity and associated second phase of $CuCr_{1-x}Mg_xO_2$ polycrystalline ceramics were also discussed. It was found that the increase of magnesium content in $CuCr_{1-x}Mg_xO_2$ polycrystalline ceramics led to the decrease of activation energy and the growth of the second-phase $MgCr_2O_4$ grains, which in turn affected the size and number of $CuCr_{1-x}Mg_xO_2$ grains. Furthermore, the electrical conductivity of $CuCr_{1-x}Mg_xO_2$ polycrystalline ceramics was affected. The results show that $CuCr_{0.6}Mg_{0.4}O_2$ polycrystalline ceramics had the smallest lattice constant c (17.083), the highest bulk density (4.367 g/cm^3), the largest average grain size (15 μm), and the smallest resistivity (0.091 Ω·cm). This is one of the best results reported so far. It has important guiding significance for the development of transparent conductive oxides with high conductivity.

References

1. A. Maignan, C. Martin, R. Frésard, V. Eyert, E. Guilmeau, S. Hébert, M. Poienar, and D. Pelloquin, Solid State Commun. 149[23-24] (2009) 962-967.
2. M.A. Marquardt, N.A. Ashmore, and D.P. Cann, Thin Solid Films. 496[1] (2006) 146-156.
3. R.S. Yu and C.M. Wu, Appl. Sur. Sci. 282 (2013) 92-97.
4. I.C. Kaya, M.A. Sevindik, and H. Akyıldız, J. Mater. Sci., Mater. Electron. 27[3] (2016) 2404-2411.
5. T. Okuda, N. Jufuku, S. Hidaka, and N. Terad, Phys. Rev. B. 72[14] (2005) 1-5.
6. Y. Tang, M. Qin, Y. Hu, K. Cui, J. Zeng, L. Chen, and L. Yu, J. Asian Ceram. Soc. 8[2] (2020) 537-541.
7. T. Okuda, Y. Beppu, Y. Fujii, T. Onoe, N. Terada, and S. Miyasaka, Phys. Rev. B. 77[13] (2008) 134423.
8. H.Y. Chen, K.P. Chang, and C.H. Yang, Appl. Sur. Sci. 273 (2013) 324-329.
9. T.S. Tripathi and M. Ka.rppinen, Adv. Electron. Mater. 3[6] (2017) 160341.
10. Y. Ono, K. Satoh, T. Nozaki, and K. Tsuyoshi, Jpn. J. Appl. Phys. 46[3A] (2007) 1071–1075.
11. Y. Wang, L. Yu, J. Wang, L. Chen, W. Gao, X. Du, and L. Biao, Mater. Lett. 75 (2012) 39-41.
12. S.K. Kurtz and F.M.A. Carpay, J. Appl. Phys. 51[11] (1980) 5725-5744.
13. T. Senda and R.C. Bradt, J. Am. Chem. Soc. 73[1] (1990) 106-114.
14. M.A. Marquardt, N.A. Ashmore, and D.P. Cann, Thin Solid Films 496[1] (2006) 146-156.
15. W. Koshibae, K. Tsutsui, and S. Maekawa, Phys. Rev. B. 62[11] (2000) 6869-6872.
16. Q. Meng, S. Lu, S. Lu, Y. Xiang. and J. Sol-Gel, Sci. Technol. 63 (2012) 1-7.
17. J.F.H.L. Monteiro, F.C. Monteiro, A.R. Jurelo, and D.H. Mosca. Ceram. Int. 44[12] (2018) 14101-14107.